

MOMENT-DRIVEN PREDICTIVE CONTROL OF MEAN-FIELD COLLECTIVE DYNAMICS*

GIACOMO ALBI[†], MICHAEL HERTY[‡], DANTE KALISE[§], AND CHIARA SEGALA[¶]

Abstract. The synthesis of control laws for interacting agent-based dynamics and their mean-field limit is studied. A linearization-based approach is used for the computation of sub-optimal feedback laws obtained from the solution of differential matrix Riccati equations. Quantification of dynamic performance of such control laws leads to theoretical estimates on suitable linearization points of the nonlinear dynamics. Subsequently, the feedback laws are embedded into nonlinear model predictive control framework where the control is updated adaptively in time according to dynamic information on moments of linear mean-field dynamics. The performance and robustness of the proposed methodology is assessed through different numerical experiments in collective dynamics.

Key words. Agent-based dynamics, mean-field equations, optimal feedback control, Riccati equations, nonlinear model predictive control

AMS subject classifications. 68Q25, 68R10, 68U05

1. Introduction. In the recent years there has been an increasing interest in the study of collective behaviour phenomena from a multiscale modelling perspective. Classical examples in socio-economy, biology and robotics are given by self-propelled particles, such animals and robots, see e.g. [2, 14, 25, 30, 52, 50, 37]. Those particles interact according to a nonlinear model encoding various social rules as for example attraction, repulsion and alignment. A particular feature of such models is their rich dynamical structure, which include different types of emerging patterns, including consensus, flocking, and milling, among many others see e.g. [44, 63, 27, 35, 58]. Understanding the impact of control inputs in such complex systems is of great relevance for applications. Results in this direction allow to design optimized actions such as collision-avoidance protocols for swarm robotics [24, 59, 60, 42], pedestrian evacuation in crowd dynamics [3, 26, 34, 19], supply chain policies [53, 28], the quantification of interventions in traffic management [64, 47, 62] or in opinion dynamics [5, 8, 43]. Here, we are concerned with the control of high-dimensional nonlinear systems of interacting particles which can describe self-organization patterns. We will consider dynamics accounting the evolution of N agents with state $v_i(t) \in \mathbb{R}^d$, undergoing a binary exchange of information weighted by a kernel $P : \mathbb{R}^d \times \mathbb{R}^d \rightarrow \mathbb{R}$ and forced by a control signal $u_i(t) \in \mathbb{R}^d$. Such dynamics can be cast in the following prototype

*Submitted to the editors DATE.

Funding: GA and CS thank the Italian Ministry of Instruction, University and Research (MIUR) to support this research with funds coming from PRIN Project 2017 (No. 2017KKJP4X entitled “Innovative numerical methods for evolutionary partial differential equations and applications”) and program Department of Excellence. GA and CS are member of the *INdAM-GNCS*. MH thanks HE5386/19,18.

[†]Department of Computer Science, University of Verona, Str. Le Grazie 15, Verona, I-37134, Italy (giacomo.albi@univr.it)

[‡]IGPM, RWTH Aachen University, Templergraben, 55, D-52062 Aachen, Germany (herty@igpm.rwth-aachen.de)

[§]School of Mathematical Sciences, University of Nottingham, University Park, Nottingham NG7 2QL, United Kingdom (dante.kalise@nottingham.ac.uk)

[¶]Department of Mathematics, University of Trento, Sommarive, Trento, Italy (chiara.segala-1@unitn.it)

model

$$(1.1) \quad \dot{v}_i = \frac{1}{N} \sum_{j=1}^N P(v_i, v_j)(v_j - v_i) + u_i =: F_i^N(v, u), \quad i = 1, \dots, N,$$

with initial data $v_i(0) = v_i^0$. While the original description of the interacting particle system such as (1.1) is based on a microscopic system of ODEs, studying the large particle limit has in many cases allowed to analyse emerging patterns or identifying relevant parameters. The derivation of a model hierarchy starting from dynamical systems to kinetic equations and fluid dynamic models has been studied intensively in the literature, for example in [16, 31, 38, 46, 29, 23]. Of particular interest for control design purposes, is the study of mean-field control approaches where the control law obtain formal independence on the number of interacting agents, [41, 39, 40, 18]. The construction of computational methods for mean-field optimal control is a challenging problem due to the nonlocality and nonlinearity arising from the interaction kernel [4, 1, 56]. Furthermore, depending on the associated cost, non-smooth and/or non-convex optimization problems might also arise [22, 12, 6].

In order to circumvent these difficulties we propose an approach where we synthesize sub-optimal feedback-type controls through the linearization of the interaction kernel and by solving the resulting linear-quadratic optimal control problem through a Riccati equation – all based on the corresponding mean-field equations, similarly as in [51, 49]. This approach also circumvents the limitations associated to the synthesis of optimal feedback laws for high-dimensional nonlinear dynamics via the Hamilton-Jacobi-Bellman PDE [33, 9]. The proposed methodology yields a control law for the linear model, which is later embedded into the non-linear model (1.1). A sketch of this control concept is given in Figure 1.1 where we show only the microscopic formulation of the model. The main advantage of the proposed design is that unlike the classical control loop (1.1, top), we do not require a continuous measurement/estimation of the nonlinear state, nor the solution to nonlinear optimal feedback law. Instead, we only require periodic measurements of the nonlinear state to update our linearized system.

However, using the linear optimal control within the nonlinear model would itself not necessarily yield a suitable control, since over time the nonlinear dynamics may be far from the linearization point. Because of the latter, we aim at quantifying the impact of this control and the number of linearization updates needed to stabilize the nonlinear system. Hence, we propose different controls, distinguishing between closed-loop and open-loop strategies: in the first case the control acts having access to the full information of the non-linear system at each time; in the second case, the control only requires information available at initial time. We quantify the performances of these control approaches estimating the decay of macroscopic quantities of system (1.1) such as its first and second moments.

In order to enhance open-loop strategies we introduce a novel Moment-driven Predictive Control (MdPC) framework. Based on dynamic estimates of the moments decay, we are able to perform a forward error analysis to estimate the next point in time where we need to update the linearization the dynamics and its feedback law. This strategy can be seen as model predictive control (MPC) technique [57, 20, 45, 10], where an open-loop control signal is applied only up to a subsequent point in time, after which the optimization is repeated. Moreover, the proposed control strategy is capable of treating efficiently high-dimensional control problems, and is robust in the case of limited access to the state and can be implemented with a small number of

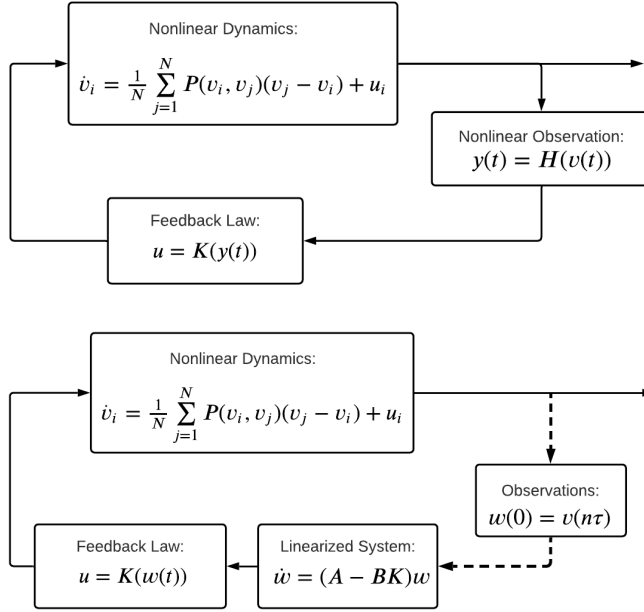


FIG. 1.1. *Top: the classical control loop for nonlinear dynamics. An (often) incomplete measurement of the state is recovered through a nonlinear observation operator, and the measurement is used to build a state estimator. This estimated state is inserted into a feedback law which requires the solution of a high-dimensional HJB PDE. This task is often unaffordable, and this block is replaced by a sub-optimal control law which is fed into the dynamics. Bottom: MdPC control methodology we propose simplifies the control loop above by requiring fewer measurements of the nonlinear state (every τ seconds), feeding this information into a linearized system for which the optimal feedback law can be easily computed.*

updates.

The paper is organized as follows in Section 2 we derive different control systems based on the linearization of the dynamics and the solution of the Riccati equation associated to the linear-quadratic optimal control problem. Section 3 is devoted to the mean-field approximation of the microscopic dynamics and presents bounds for the moments decay. In Section 4 the Moment-driven Predictive Control framework is described and two different implementations are presented. Finally, in Section 5 we assess the proposed design via numerical experiments, showing different applications in the context of opinion formation and alignment dynamics.

2. Control of an interacting multi-agent system. In this section we present a linearization-based approach for the control of large-scale interacting particle systems. We are concerned with the evolution of N interacting agents, whose states $v_i(t) \in \mathbb{R}^d$ evolve according to the following nonlinear model

$$(2.1) \quad \dot{v}_i = \frac{1}{N} \sum_{j=1}^N P(v_i, v_j)(v_j - v_i) + u_i, \quad v_i(0) = v_i^0, \quad i = 1, \dots, N,$$

where $P : \mathbb{R}^d \times \mathbb{R}^d \rightarrow \mathbb{R}$ denotes an interaction kernel among agents, which is in general a nonlinear function. Further assumptions regarding the interaction kernel will be discussed in the forthcoming sections. The term $u_i \in \mathbb{R}^d$ represents an external

control variable acting over the i -th agent of the system. The complete set of control variables is denoted by $u = (u_1, \dots, u_N) \in \mathbb{R}^{N \times d}$. In order to synthesize this control variable, we assume that u is the minimizer of a cost function $J(u; v(0))$, that is

$$(2.2) \quad u^* = \arg \min_u J(u; v^0) := \int_0^T \ell(v(t), u(t)) dt, \quad \text{subject to (2.1)}.$$

The optimization horizon T expresses the time scale along which we minimize the running cost $\ell(v, u)$, encodes our objective as a function of the state and control variables. In the context of this work, we are interested in *consensus equilibrium*, namely, reaching a consensus velocity $\tilde{v} \in \mathbb{R}^d$ such that $v_1 = \dots = v_N = \tilde{v}$. With a slight abuse of notation, we shall denote indistinctively by \tilde{v} the consensus state and the swarm configuration $\tilde{v} \in \mathbb{R}^{N \times d}$ where all the agents share the same velocity. In order to promote consensus emergence, we solve the optimal control problem (2.2) to determine a control law u driving the system towards \tilde{v} using the running cost

$$(2.3) \quad \ell(v, u) = \frac{1}{N} \sum_{j=1}^N (|v_j - \tilde{v}|^2 + \nu |u_j|^2)$$

where $\nu > 0$ is a penalization parameter for the control energy, and \tilde{v} is a prescribed consensus point. The norm $|\cdot|$ is the usual Euclidean norm in \mathbb{R}^d .

2.1. Linearization and the LQR approach for collective dynamics. We are interested in the synthesis of a feedback control law for the control of the nonlinear dynamics (2.1). We begin by defining the vector-valued function $F(v) : \mathbb{R}^{N \times d} \rightarrow \mathbb{R}^{N \times d}$ such that

$$(2.4) \quad F_i(v) = \frac{1}{N} \sum_{j=1}^N P(v_i, v_j)(v_j - v_i), \quad i = 1, \dots, N.$$

We linearize the dynamics around $v_i = \bar{v}$ for every agent, which corresponds to an arbitrary equilibrium for the nonlinear dynamics (2.1), i.e. $F(\bar{v}) = 0$. We further assume that the communication function $P(v_i, v_j)$ is such that

$$(2.5) \quad P(\bar{v}, \bar{v}) \equiv \bar{p},$$

with \bar{p} a bounded value. Computing the first order approximation of $F(v)$ around \bar{v} , we have

$$(2.6) \quad \nabla_v F(\bar{v})(v - \bar{v}) = A(v - \bar{v}),$$

where $A \in \mathbb{R}^{N \times N}$ is the Laplacian matrix defined as follows

$$(2.7) \quad (A)_{ij} = \begin{cases} a_d = \frac{\bar{p}(1-N)}{N}, & i = j, \\ a_o = \frac{\bar{p}}{N}, & i \neq j. \end{cases}$$

We observe that the structure of matrix A is such that $A(v - \bar{v}) = Av$ since \bar{v} is a consensus point. To write the linearized system associated to (2.1) we further consider the change of variables $w_i(t) := v_i(t) - \bar{v}$, and we have

$$(2.8) \quad \dot{w}_i = \frac{1}{N} \sum_{j=1}^N \bar{p}(w_j - w_i) + u_i, \quad w_i(0) = v_i^0 - \bar{v}.$$

For the linearized dynamics we cast as the *Linear Quadratic Regulator* (LQR) control problem, where the functional (2.2) reads as follows

$$(2.9) \quad J(u, w(0)) = \int_0^T w^\top Q w + \nu u^\top R u dt$$

in the matrix-vector notation with $w = (w_1, \dots, w_N)$ and matrices $Q \equiv R = \frac{1}{N} \text{Id} \in \mathbb{R}^{N \times N}$. The linear dynamics (2.8) are equivalent to

$$(2.10) \quad \dot{w} = Aw + Bu, \quad w(0) = v^0 - \bar{v},$$

where $B = \text{Id} \in \mathbb{R}^{N \times N}$ is the identity matrix.

LEMMA 2.1. *The pair (A, B) in the dynamics (2.8) is controllable for any consensus state \bar{v} .*

Proof. Since the control operator $B = \text{Id}$ it follows directly that the controllability matrix

$$(2.11) \quad C(A, B) = [B; AB; \dots; A^{N-1}B] = [\text{Id}; A; \dots; A^{N-1}],$$

has $\text{rank}(C) = N$. □

This result straightforwardly implies that in a neighbourhood of any constant state \bar{v} the non linear system (2.1) admits a continuous stabilizing feedback, see for example [17].

In order to synthesize a stabilizing control law we solve the optimal control problem (2.9)–(2.10), whose exact solution is given in feedback form by

$$(2.12) \quad u(t) = -\frac{N}{\nu} K(t)w(t)$$

with $K(t) \in \mathbb{R}^{N \times N}$ fulfilling the Differential Riccati matrix-equation

$$(2.13) \quad -\dot{K} = KA + A^\top K - \frac{N}{\nu} KK + Q, \quad K(T) = 0 \in \mathbb{R}^{N \times N},$$

coupled to the evolution of the controlled system

$$\dot{w}(t) = Aw(t) - \frac{N}{\nu} K(t)w(t).$$

For a general linear system we need to solve the $N \times N$ differential system (2.13), which can be costly for large-scale agent-based dynamics. However, in this case we can exploit the symmetric structure of the Laplacian matrix A to reduce the Riccati equation.

PROPOSITION 2.2 (Properties of the Differential Riccati Equation). *Consider the linear dynamics (2.8), the solution of the Riccati equation (2.13) can be reduced to the solution of two coupled equations*

$$(2.14a) \quad -\dot{k}_d = 2k_d a_d + 2(N-1)k_o a_o - \frac{N}{\nu} (k_d^2 + (N-1)k_o^2) + \frac{1}{N}, \quad k_d(T) = 0,$$

$$(2.14b) \quad -\dot{k}_o = 2(N-2)k_o a_o + 2k_o a_d + 2k_d a_o - \frac{N}{\nu} (2k_d k_o + (N-2)k_o^2), \quad k_o(T) = 0.$$

such that

$$(K)_{ij} = \begin{cases} k_d, & i = j, \\ k_o, & i \neq j. \end{cases}$$

Proof. Given the structure of the matrices K , A and Q , solving the Riccati equation (2.13) componentwise leads to the following identities:

For the diagonal entries k_{ii} we have

$$\begin{aligned} (KA + A^\top K)_{ii} &= 2(KA)_{ii} = 2k_d a_d + 2(N-1)k_o a_o, \\ \frac{N}{\nu}(K^2)_{ii} &= \frac{N}{\nu}(k_d^2 + (N-1)k_o^2). \end{aligned}$$

For the off-diagonal entries $i \neq j$, we find

$$\begin{aligned} (KA + A^\top K)_{ij} &= 2(N-2)k_o a_o + 2k_o a_d + 2k_d a_o, \\ \frac{N}{\nu}(K^2)_{ij} &= \frac{N}{\nu}(2k_d k_o + (N-2)k_o^2). \end{aligned}$$

Summing up these terms we obtain the structure of K . \square

We can further simplify the Riccati-matrix system (2.14) using the dependency of coefficients a_d, a_o (2.7) and the parameter \bar{p} . This leads to

$$(2.15) \quad -\dot{k}_d = -\frac{2\bar{p}(N-1)}{N}(k_d - k_o) - \frac{N}{\nu}(k_d^2 + (N-1)k_o^2) + \frac{1}{N}, \quad k_d(T) = 0,$$

$$(2.16) \quad -\dot{k}_o = \frac{2\bar{p}}{N}(k_d - k_o) - \frac{N}{\nu}(2k_d k_o + (N-2)k_o^2), \quad k_o(T) = 0.$$

Since we are interested in the dynamics for large number of agents, we introduce the following scalings

$$(2.17) \quad k_d \leftarrow N k_d, \quad k_o \leftarrow N^2 k_o, \quad \alpha(N) = \frac{N-1}{N}.$$

For simplicity we keep the same notation also for the scaled variables k_d, k_o .

Under this scaling the system (2.15)–(2.16) reads

$$(2.18) \quad -\dot{k}_d = -2\bar{p}\alpha(N) \left(k_d - \frac{k_o}{N} \right) - \frac{1}{\nu} \left(k_d^2 + \frac{\alpha(N)}{N} k_o^2 \right) + 1, \quad k_d(T) = 0,$$

$$(2.19) \quad -\dot{k}_o = 2\bar{p} \left(k_d - \frac{k_o}{N} \right) - \frac{1}{\nu} \left(2k_d k_o + \alpha(N) k_o^2 - \frac{1}{N} k_o^2 \right), \quad k_o(T) = 0,$$

and the Riccati feedback law (2.12) is obtained as follows

$$(2.20) \quad u_i = -\frac{1}{\nu} \left(\left(k_d - \frac{k_o}{N} \right) w_i(t) + \frac{k_o}{N} \sum_{j=1}^N w_j(t) \right).$$

Plugging the control into the linear dynamics (2.8) and rearranging the terms we have

$$(2.21) \quad \dot{w}_i = \left(\bar{p} - \frac{\tilde{k}_o}{\nu} \right) \frac{1}{N} \sum_{j=1}^N w_j - \left(\bar{p} + \frac{k_d}{\nu} - \frac{k_o}{\nu N} \right) w_i, \quad w_i(0) = v_i^0 - \bar{v}.$$

The controlled dynamics (2.21) are non-autonomous as the coefficients $\tilde{k}_d(t), \tilde{k}_o(t)$, have to be determined offline by solving (2.18)–(2.19) backwards in time.

In order to analyse the large-scale behaviour of the system we introduce the average of the agent states, and a weighted combination of the Riccati coefficients, respectively

$$m_w^N(t) := \frac{1}{N} \sum_{j=1}^N w_j(t), \quad s(t) := k_d(t) + \alpha(N)k_o(t).$$

From (2.21), (2.18) and (2.19) we get the following system for the evolution of $m_w^N(t)$ and $s(t)$, respectively:

$$(2.22) \quad \begin{aligned} \dot{m}_w^N(t) &= -\frac{1}{\nu} s(t) m_w^N(t), & m_w^N(0) &= m_w^N(0) - \bar{v}, \\ -\dot{s}(t) &= 1 - \frac{1}{\nu} s(t)^2, & s(T) &= 0. \end{aligned}$$

The second equation has an explicit solution $s(t) = \sqrt{\nu} \tanh((T-t)/\sqrt{\nu})$, always non-negative for $t \in [0, T]$ as already observed in [51]. Therefore the average $m_w^N(t)$ follows a relaxation process towards the state \bar{v} , as follows

$$(2.23) \quad \dot{m}_v^N(t) = -\frac{1}{\sqrt{\nu}} \tanh\left(\frac{T-t}{\sqrt{\nu}}\right) (m_v^N(t) - \bar{v}).$$

Remark 2.1 (Second order dynamics). This approach can be extended to second order models [27, 35, 58]. Here, the state space of a swarm of N agents is characterized described by position and velocities $(x_i(t), v_i(t))_i \in \mathbb{R}^{2 \times d}$, evolving according to

$$(2.24) \quad \begin{aligned} \dot{x}_i &= v_i, & i &= 1, \dots, N \\ \dot{v}_i &= \frac{1}{N} \sum_{j=1}^N P(x_i, x_j) (v_j - v_i) + u_i, \end{aligned}$$

where $u \in \mathbb{R}^{N \times d}$. We consider again a functional of type (2.3), where we enforce a consensus point $v_i = v_j = \tilde{v}$ for every i, j . Linearizing around this point and introducing the shift

$$y_i = x_i - \bar{v}t, \quad w_i = v_i - \bar{v}$$

we have stabilization

$$(2.25) \quad \begin{bmatrix} \dot{y} \\ \dot{w} \end{bmatrix} = \begin{bmatrix} 0 & \text{Id} \\ 0 & A \end{bmatrix} \begin{bmatrix} y \\ w \end{bmatrix} + \begin{bmatrix} 0 \\ \text{Id} \end{bmatrix} u.$$

This augmented system is controllable [49], and the associated differential Riccati-matrix equation reads

$$(2.26) \quad \begin{aligned} \begin{bmatrix} \dot{K}_{11} & \dot{K}_{12} \\ \dot{K}_{21} & \dot{K}_{22} \end{bmatrix} &= \begin{bmatrix} 0 & 0 \\ 0 & K_{21} + K_{22}A \end{bmatrix} + \begin{bmatrix} 0 & 0 \\ K_{11} + AK_{21} & K_{12} + AK_{22} \end{bmatrix} \\ &\quad - \frac{N}{\nu} \begin{bmatrix} K_{12}K_{21} & K_{12}K_{22} \\ K_{22}K_{21} & (K_{22})^2 \end{bmatrix} + \begin{bmatrix} 0 & 0 \\ 0 & \text{Id} \end{bmatrix}, \end{aligned}$$

with terminal conditions $K_{ij}(T) = 0$, for $i, j = 1, 2$. The system can be solved by $K_{11} = K_{12} = K_{21} = 0$ and

$$-\dot{K}_{22} = K_{22}A + AK_{22} - \frac{N}{\nu} (K_{22})^2 + \text{Id}, \quad K_{22} = 0.$$

The latter equation is equivalent to equation (2.13). Hence, the results we obtain for the first order system can be extended to second order systems. We will further discuss this extension in the numerical section.

2.2. Riccati-based control laws for the non-linear system. In order to approximate the synthesis of optimal feedback laws for the original nonlinear optimal control problem (2.2), we study sub-optimal stabilizing strategies induced by the Riccati control (2.12). Without loss of generality, we will consider the stabilization problem towards $\tilde{v} = 0$. Consider the following functional

$$(2.27) \quad \min_u J(u; v^0) := \int_0^T \frac{1}{N} \sum_{j=1}^N (|v_j|^2 + \nu |u_j|^2) dt, \quad \text{subject to} \quad (2.1).$$

We will focus on different ways to synthesize a control law based on the information retrieved in the linearized case: a closed-loop control, an open-loop strategy, and a simplified inexact open-loop control.

Closed-loop control. A well-known local strategy for the control of nonlinear dynamics is to use the optimal feedback control obtained from the linearized dynamics. In this case, the controlled system reads

$$(2.28) \quad \dot{v}_i = \frac{1}{N} \sum_{j=1}^N P(v_i, v_j)(v_j - v_i) + R_i[v](t), \quad v_i(0) = v_i^0,$$

where the operator $R_i[\cdot]$ is the feedback (2.12) applied directly to the state of the non-linear system $v(t) = (v_i(t))_{i=1}^N$, namely

$$(2.29) \quad R_i[v](t) = -\frac{1}{\nu} \left(\left(k_d(t) - \frac{k_o(t)}{N} \right) v_i(t) + \frac{k_o(t)}{N} \sum_{j=1}^N v_j(t) \right),$$

where $k_o(t), k_d(t)$ are still obtained as solution of system (2.19)–(2.18). In general, such a control law is expected to work only for initial states sufficiently close to the state around which the dynamics have been linearised. We shall investigate in detail the properties of the closed-loop in the following section.

Open-loop control. The open-loop strategy we propose applies the control signal obtained from the linear synthesis $u_i(t; v^0)$ directly into the the non-linear dynamics as follows

$$(2.30) \quad \begin{aligned} \dot{v}_i &= \frac{1}{N} \sum_{j=1}^N P(v_i, v_j)(v_j - v_i) + R_i[w](t), & v_i(0) &= v_i^0, \\ \dot{w}_i &= \frac{1}{N} \sum_{j=1}^N \bar{p}(w_j - w_i) + R_i[w](t), & w_i(0) &= v_i^0, \end{aligned}$$

where the control $R_i[w](t)$ is computed according to (2.12), namely

$$(2.31) \quad R_i[w](t) = -\frac{1}{\nu} \left(\left(k_d(t) - \frac{k_o(t)}{N} \right) w_i(t) + \frac{k_o(t)}{N} \sum_{j=1}^N w_j(t) \right),$$

with $k_o(t), k_d(t)$ obtained solving the system (2.19)–(2.18). This approach is open-loop, since all the information on the state of the non-linear system is cast into the initial state of linearized system, assuming $w_i^0 = v_i^0$. While this approach is clearly outperformed by the closed-loop feedback law in terms of robustness, it has the advantage that it can be implemented without requiring a continuous measurement of the full nonlinear state $v(t)$, and making it appealing for systems where recovering the true state of the dynamics can be expensive or time-consuming.

Inexact open-loop control. An inexact, but simpler, implementation of the open-loop approach (2.30) obtained when the control $R_i[\cdot]$ is evaluated only with respect to the initial data v_i^0 is

$$(2.32) \quad R_i[v^0](t) = -\frac{1}{\nu} \left(\left(k_d(t) - \frac{k_o(t)}{N} \right) v_i^0 + \frac{k_o(t)}{N} \sum_{j=1}^N v_j^0 \right).$$

This setting avoids the evaluation of system in (2.30) reducing to the computation of

$$(2.33) \quad \dot{v}_i = \frac{1}{N} \sum_{j=1}^N P(v_i, v_j)(v_j - v_i) + R_i[v^0](t), \quad v_i(0) = v_i^0.$$

The open-loop control laws are meant to be embedded in a Model Predictive Control framework, ensuring a sufficiently frequent update of the state of the nonlinear system ensuring stability of the resulting control system. This shall be further analysed in Section 4.

In the following section we will study the impact of these control strategies for the stabilization of the non-linear dynamics in the case of large number of agents $N \gg 1$.

3. Mean field limits and moments estimates. The stabilization strategies (2.28) and (2.30) are clearly suboptimal with respect to the original optimal control problem, and in general will not guarantee the stabilization of the non-linear dynamics (2.1). In this section we want to quantify the discrepancy between the desired target state and the final state obtained by the stabilization strategies (2.28) and (2.30). In order to estimate these performances in the case where a large number of agents is present, i.e. $N \gg 1$, we discuss our approaches in the *mean-field limit*. Hence we consider density distribution of agents in order to describe the collective behavior.

In this scale we retrieve upper and lower bounds for the decay of the mean-field density towards the desired configuration for different approaches.

3.1. Open-loop Riccati control. The empirical joint probability distribution of particles of system (2.1) and (2.8)

$$(3.1) \quad \lambda^N(v, w, t) = \frac{1}{N} \sum_{i=1}^N \delta(v - v_i(t)) \delta(w - w_i(t)),$$

where $\delta(\cdot)$ is a Dirac measure. For the microscopic models we assume enough regularity on interaction kernel, such that particles remain in a fixed compact domain for all N and in the whole time interval $[0, T]$. We refer to [21, 23] for a rigorous treatment of the mean-field limit of interacting particle systems. Hence we introduce the test function $\phi(v, w) \in C_0^1(\mathbb{R}^{2d})$ and by Liouville's theorem we compute the time variation of the inner-product $\langle \lambda^N(t), \phi \rangle$, as follows

$$(3.2) \quad \frac{d}{dt} \langle \lambda^N(t), \phi \rangle = \frac{1}{N} \sum_{i=1}^N (\nabla_v \phi(v_i, w_i) \cdot \dot{v}_i(t) + \nabla_w \phi(v_i, w_i) \cdot \dot{w}_i(t)),$$

We denote by $\lambda^N(t) := \lambda^N(v, w, t)$ and we use the marginal density f^N, g^N and the average $m_1[f^N]$ defined as follows

(3.3)

$$\begin{aligned} f^N(w, t) &:= \int_{\mathbb{R}^d} \lambda^N(v, w, t) dv = \frac{1}{N} \sum_{i=1}^N \delta(w - w_i(t)), \\ g^N(v, t) &:= \int_{\mathbb{R}^d} \lambda^N(v, w, t) dw = \frac{1}{N} \sum_{i=1}^N \delta(v - v_i(t)), \quad m_1[f^N](t) := \int_{\mathbb{R}^d} w f^N(w, t) dw. \end{aligned}$$

We define $\mathcal{P}[g]$ the nonlocal integral

$$\mathcal{P}[g](v, t) = \int_{\mathbb{R}^d} P(v, v_*) (v_* - v) g(v_*, t) dv_*.$$

With the standard derivation of the mean field limit, we obtain in the strong form the evolution equation for $\lambda^N(v, w, t)$ as follows

$$\begin{aligned} \partial_t \lambda^N &= -\nabla_v \cdot [\lambda^N (\mathcal{P}[g^N] - a^N(t)w - b^N(t)m_1[f^N])] \\ &\quad - \nabla_w \cdot [\lambda^N (\bar{p}(m_1[f] - w) - a^N(t)w - b^N(t)m_1[f^N])], \end{aligned}$$

coupled with the evolution of the Riccati system through the coefficients $a^N(t)$ and $b^N(t)$

$$\begin{aligned} -\dot{k}_d &= -2\bar{p}\alpha(N) \left(k_d - \frac{k_o}{N} \right) - \frac{1}{\nu} \left(k_d^2 + \frac{\alpha(N)}{N} k_o^2 \right) + 1, & k_d(T) &= 0, \\ -\dot{k}_o &= 2\bar{p} \left(k_d - \frac{k_o}{N} \right) - \frac{1}{\nu} \left(2k_d k_o + \alpha(N) k_o^2 - \frac{1}{N} k_o^2 \right), & k_o(T) &= 0. \end{aligned}$$

Since we are interested in the limit of a large number of agents, for $N \rightarrow \infty$ we have

$$\lim_{N \rightarrow \infty} a^N(t) = \frac{k_d(t)}{\nu}, \quad \lim_{N \rightarrow \infty} b^N(t) = \frac{k_o(t)}{\nu},$$

where k_d and k_o fulfill

$$\begin{aligned} (3.4) \quad -\dot{k}_d &= -2\bar{p}k_d - \frac{k_d^2}{\nu} + 1, & k_d(T) &= 0 \\ -\dot{k}_o &= 2\bar{p}k_d - \frac{k_o}{\nu} (2k_d + k_o), & k_o(T) &= 0. \end{aligned}$$

Then the joint mean-field model can be conveniently written

$$\begin{aligned} (3.5) \quad \partial_t \lambda &= -\nabla_v \cdot \left[\lambda \left(\mathcal{P}[g] - \frac{k_d}{\nu} w - \frac{k_o}{\nu} m_1[f] \right) \right] \\ &\quad - \nabla_w \cdot \left[\lambda \left(\bar{p}(m_1[f] - w) - \frac{k_d}{\nu} w - \frac{k_o}{\nu} m_1[f] \right) \right], \end{aligned}$$

with initial data $\lambda(v, w, 0) = \lambda^0(v, w)$. Integrating the mean-field equation (3.5) with respect to the v and w we derive the evolution of the marginals $f(w, t)$ and $g(v, t)$. We obtain the following system

$$(3.6a) \quad \partial_t g = -\nabla_v \cdot \left[g \left(\mathcal{P}[g] - \frac{k_d}{\nu} m_1[h] - \frac{k_o}{\nu} m_1[f] \right) \right], \quad g(v, 0) = g^0(v)$$

$$(3.6b) \quad \partial_t f = -\nabla_w \cdot \left[f \left(\left(\bar{p} - \frac{k_o}{\nu} \right) m_1[f] - \left(\bar{p} + \frac{k_d}{\nu} \right) w \right) \right], \quad f(w, 0) = g^0(w)$$

with $m_1[h](v, t)$ being the average of the conditional probability $h(w|v, t)$ defined as

$$(3.7) \quad \lambda(t, v, w) = h(t, w|v)g(t, v), \quad m_1[h](t, v) = \int_{\mathbb{R}^d} wh(t, w|v)dw.$$

We observe that equation (3.6b) of system (3.6), is the mean field equation associated to the linear controlled model (2.21),[51]. On the other hand the mean-field equation for the non-linear model (3.6a) is coupled to the solution of the linear model through the control action.

Remark 3.1 (Inexact mean-field open-loop control). If we consider the inexact open-loop control (2.33)–(2.32), where the control acts only on the information gathered at the initial time t_0 , we derive a consistent mean-field limit following the procedure described in this section. Thus the evolution of the joint distribution $\lambda(v, w, t)$ reads

$$(3.8) \quad \partial_t \lambda = -\nabla_v \cdot \left[\lambda \left(\mathcal{P}[g] - \frac{k_d}{\nu} w - \frac{k_o}{\nu} m_1[g^0] \right) \right], \quad \lambda(v, w, 0) = \lambda^0(v, w).$$

The marginal distributions of $\lambda(v, w, t)$ corresponds to the initial data $g^0(w)$ and $g(v, t)$ respectively, the system (3.6) reduces then to the equation

$$(3.9) \quad \partial_t g = -\nabla_v \cdot \left[g \left(\mathcal{P}[g] - \frac{k_d}{\nu} m_1[h] - \frac{k_o}{\nu} m_1[g^0] \right) \right], \quad g(v, 0) = g^0(v).$$

3.1.1. Bounds of decay moments. We are interested in the evolution of the first and second moments of the nonlinear mean field density $g(v, t)$, namely

$$m_1[g](t) = \int_{\mathbb{R}^d} vg(t, v) dv, \quad m_2[g](t) = \int_{\mathbb{R}^d} |v|^2 g(t, v) dv.$$

Stabilizing the system at target consensus point $\bar{v} = 0$ requires estimates on the decay of moments towards zero. Performing the analysis we assume the kernel $P(\cdot, \cdot)$ to be a symmetric and bounded function, namely

$$(A) \quad P(v, v_*) = P(v_*, v), \quad P(v, v_*) \in [-a, b], \quad \forall v, v_* \in \mathbb{R}^d, \quad a, b \geq 0.$$

Observing model (3.6) the initial averages are identical $m_1[f^0] = m_1[g^0]$, moreover we show that under assumption (A) we have

$$m_1[f](t) \equiv m_1[g](t), \quad t \geq 0.$$

Indeed, computing the evolution of $m_1[f](t)$ from (3.6b), we have

$$(3.10) \quad \frac{d}{dt} m_1[f](t) = -\frac{k_d + k_o}{\nu} m_1[f](t), \quad m_1[f](0) = m_1[g^0], .$$

This equation coincides with equation (2.22). The first moment of $g(v, t)$ fulfills

$$\begin{aligned} \frac{d}{dt} m_1[g] &= \int_{\mathbb{R}^{2d}} P(v, v_*) (v_* - v) g g_* dv dv_* - \frac{k_d}{\nu} \int_{\mathbb{R}^d} m_1[h](v) g dv - \frac{k_o}{\nu} m_1[f] \\ &= \int_{\mathbb{R}^{2d}} (vP(v_*, v) - vP(v, v_*)) g g_* dv dv_* - \frac{k_d}{\nu} \int_{\mathbb{R}^{2d}} wh(w|v)g(v) dv dw - \frac{k_o}{\nu} m_1[f] \\ &= -\frac{k_d}{\nu} \int_{\mathbb{R}^{2d}} w \lambda(v, w) dv dw - \frac{k_o}{\nu} m_1[f] = -\frac{k_d + k_o}{\nu} m_1[f], \end{aligned}$$

where we omitted time dependencies and we indicate with gg_* the product of $g(t, v)$ and $g(t, v_*)$. The last two equalities follow from the symmetry of $P(\cdot)$ and the definition of joint distribution.

The second moment of $g(v, t)$ is obtained by (3.6a), as

$$\begin{aligned} \frac{d}{dt}m_2[g] &= 2 \int_{\mathbb{R}^{2d}} v \cdot (v - v_*) P(v, v_*) gg_* dv dv_* - 2 \frac{k_o}{\nu} m_1[f] m_1[g] - 2 \frac{k_d}{\nu} \int_{\mathbb{R}^{2d}} v w h(w|v) g(v) dv dw \\ &= - \int_{\mathbb{R}^{2d}} |v - v_*|^2 P(v, v_*) gg_* dv dv_* - 2 \frac{k_o}{\nu} m_1[f] m_1[g] - 2 \frac{k_d}{\nu} \int_{\mathbb{R}^{2d}} v w \lambda(v, w) dv dw \\ &= - \int_{\mathbb{R}^{2d}} |v - v_*|^2 P(v, v_*) gg_* dv dv_* - 2 \frac{k_d + k_o}{\nu} (m_1[g])^2 - 2 \frac{k_d}{\nu} \varrho[f, g] \sqrt{\sigma^2[f] \sigma^2[g]} \end{aligned} \quad \blacksquare$$

where in the last equality we used $m_1[g] \equiv m_1[f]$ and

$$\int_{\mathbb{R}^{2d}} v w \lambda(v, w) dv dw = \varrho[f, g] \sqrt{\sigma^2[f] \sigma^2[g]} + m_1[f] m_1[g],$$

with $-1 \leq \varrho[f, g] \leq 1$ the correlation coefficient between f and g , $\sigma^2[f]$, $\sigma^2[g]$ are their variances. By observing that

$$(3.11) \quad \frac{d}{dt} (m_1[g])^2 = -2 \frac{k_d + k_o}{\nu} (m_1[g])^2$$

and using the definition of the variance $\sigma^2[g] = m_2[g] - |m_1[g]|^2$ we can rewrite the equation as the following differential equation

$$(3.12) \quad \frac{d}{dt} \sigma^2[g] = - \int_{\mathbb{R}^{2d}} |v - v_*|^2 P(v, v_*) gg_* dv dv_* - 2 \frac{k_d}{\nu} \varrho \sqrt{\sigma^2[f] \sigma^2[g]}.$$

For the sake of completeness we derive also the equation for the evolution of second moment of f :

$$\begin{aligned} \frac{d}{dt} m_2[f] &= 2\bar{p} \int_{\mathbb{R}^{2d}} w \cdot (w - w_*) f f_* dw dw_* - 2 \frac{k_o}{\nu} m_1[f] \int_{\mathbb{R}^d} w f(w) dw - 2 \frac{k_d}{\nu} \int_{\mathbb{R}^d} |w|^2 f(w) dw \\ &= -2\bar{p} \int_{\mathbb{R}^{2d}} |w - w_*|^2 f f_* dw dw_* - 2 \frac{k_o}{\nu} |m_1[f]|^2 - 2 \frac{k_d}{\nu} m_2[f]. \end{aligned} \quad \blacksquare$$

Eventually, adding and subtracting $2k_d/\nu(m_1[f])^2$ to the right hand side of the last equation and taking into account the following identity

$$(3.13) \quad \int_{\mathbb{R}^{2d}} |w - w_*|^2 f f_* dw dw_* = 2\sigma^2[f] = 2m_2[f] - 2|m_1[f]|^2.$$

Leads to the following differential equation for the variance $\sigma^2[f]$:

$$(3.14) \quad \frac{d}{dt} \sigma^2[f] = -2 \left(2\bar{p} + \frac{k_d}{\nu} \right) \sigma^2[f],$$

with initial data $\sigma^2[f^0] \equiv \sigma^2[g^0]$.

PROPOSITION 3.1. *Under assumption (A) on the interaction kernel $P(\cdot)$, we have the following lower and upper bound for the evolution of the variance $\sigma^2[g]$*

$$(3.15) \quad \sigma^2[g^0] e^{-2bt} (1 - B_b^+(0, t))^2 \leq \sigma^2[g](t) \leq \sigma^2[g^0] e^{2at} (1 + B_a^-(0, t))^2,$$

where

$$(3.16) \quad \begin{aligned} B_c^\pm(t_0, t) &= \frac{1}{\nu} \int_{t_0}^{t-t_0} \beta(s-t_0) k_d(s) e^{\pm c(s-t_0)} ds, \\ \beta(t-t_0) &= \exp \left\{ -2\bar{p}(t-t_0) - \frac{1}{\nu} \int_{t_0}^{t-t_0} k_d(r) dr \right\}. \end{aligned}$$

Proof. Consider the case first $P(v, w) \geq -a$. We bound from below the interaction kernel in equation (3.12),

$$\begin{aligned} \frac{d}{dt} \sigma^2[g](t) &\leq 2a \int_{\mathbb{R}^{2d}} |v-v_*|^2 g g_* dv dv_* - 2 \frac{k_d}{\nu} \varrho \sqrt{\sigma^2[f] \sigma^2[g]} \\ &\leq 2a \sigma^2[g] - 2 \frac{k_d}{\nu} \sqrt{\sigma^2[f] \sigma^2[g]}. \end{aligned}$$

where we first used the identity (3.13) and $|\varrho| \leq 1$. In order to estimate the growth of the right hand side we note that $\sigma[f](t)$ by (3.14), is given as

$$\sigma^2[f](t) = \sigma^2[g^0] \exp \left\{ -4\bar{p}t - \frac{2}{\nu} \int_0^t k_d(s) ds \right\} =: \sigma^2[g^0] \beta(t)^2.$$

Substituting the estimate in the previous equation we obtain

$$\frac{d}{dt} \sigma^2[g](t) \leq 2a \sigma^2[g](t) + \frac{2k_d}{\nu} \beta(t) \sqrt{\sigma^2[g^0] \sigma^2[g](t)}.$$

An estimate can be obtained for $z \neq 0$:

$$\frac{d}{dt} z(t) = az(t) + \frac{k_d}{\nu} \beta(t) \sqrt{\sigma^2[g^0]}.$$

This first order linear differential equation admit an exact solution as follows

$$(3.17) \quad z(t) = z(0) e^{at} \left(1 + \frac{1}{\nu} \int_0^t e^{-as} k_d(s) \beta(s) ds \right).$$

Applying the Petrovitsch's theorem [61] we obtain the upper variance bound.

$$(3.18) \quad \sigma^2[g](t) \leq \sigma^2[g^0] e^{2at} \left(1 + \frac{1}{\nu} \int_0^t e^{-as} k_d(s) \beta(s) ds \right)^2.$$

For case $P(v, w) \leq b$. Bounding from above $P(\cdot, \cdot)$ in (3.12) we have the differential inequality

$$\begin{aligned} \frac{d}{dt} \sigma^2[g](t) &\geq -2b \sigma^2[g](t) - 2 \frac{k_d}{\nu} \varrho \sqrt{\sigma^2[f] \sigma^2[g]} \\ &\geq -2b \sigma^2[g](t) - 2 \frac{k_d}{\nu} \sqrt{\sigma^2[f] \sigma^2[g]}. \end{aligned}$$

Solving exactly (3.14), and substituting $\sigma[f](t)$ into the previous equation

$$\frac{d}{dt} \sigma^2[g](t) \geq -2b \sigma^2[g](t) - \frac{2k_d}{\nu} \beta(t) \sqrt{\sigma^2[g^0] \sigma^2[g](t)}.$$

Proceeding as in equation (3.17) we obtain

$$(3.19) \quad \sigma^2[g](t) \geq \sigma^2[g^0] e^{-2bt} \left(1 - \frac{1}{\nu} \int_0^t e^{bs} k_d(s) \beta(s) ds \right)^2. \quad \square$$

In Figure 3.2 two examples for the decay of the variance $\sigma^2[g]$ and the bounds associated to the kernel are shown.

$$(3.20) \quad P(v, w) = \alpha + \frac{K}{(\varsigma + |v - w|^2)^\gamma}, \quad \alpha, \varsigma, \gamma \geq 0, \text{ and } K \in \mathbb{R}.$$

On the left we consider the attractive case, where $P(\cdot)$ is positive, and bounded in $[0, 1]$ with $\alpha = 0, \varsigma = 1, K = 1$ and $\gamma = 2$. This is the Cucker-Smale kernel [27]. On the right we show an attraction-repulsion dynamics with kernel $-1 \leq P(\cdot, \cdot) \leq 9$ where $\alpha = 9, \varsigma = 0.1, K = -1$ and $\gamma = 1$. The value of σ_g^2 is computed integrating numerically a mean field approximation of the nonlinear dynamic equation. In both cases, the initial density of particle $g^0(v)$ is

$$g^0(v) = \frac{2}{3} \chi_{[1/4, 7/4]}(v).$$

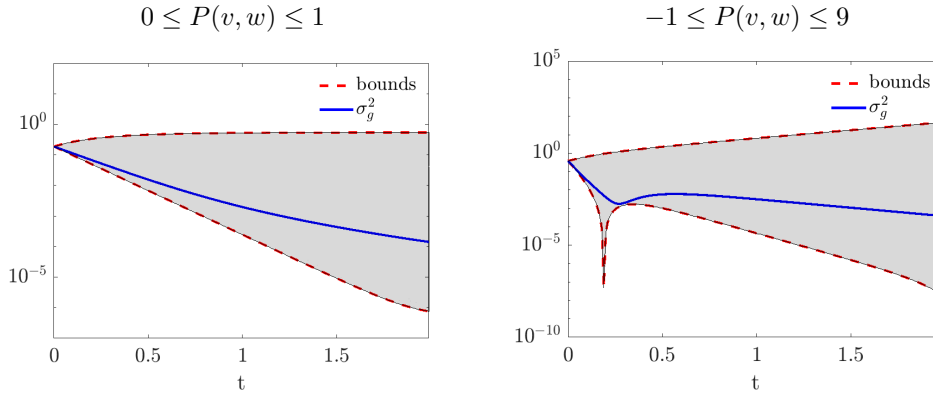


FIG. 3.2. Variance decay and bounds for the open-loop approach (2.30). On the left we observe the decay for an attractive dynamics, on the right the attractive-repulsive case.

Remark 3.2 (Bounds for inexact open-loop Riccati control). For the inexact open-loop Riccati control we observe that bounds on moments can be computed in similar fashion by the mean-field model (3.9). The first moment (3.9) is given by

$$(3.21) \quad \frac{d}{dt} m_1[g](t) = -\frac{k_d(t) + k_o(t)}{\nu} m_1[g^0], \quad m_1[g](0) = m_1[g^0].$$

A substantial difference with respect to the exponential decay of the average (3.10) is observed since the exact solution to (3.21) is

$$(3.22) \quad m_1[g](t) = m_1[g^0] \left(1 - \frac{1}{\nu} \int_0^t (k_d(s) + k_o(s)) ds \right).$$

Bounds of the variance of $g(v, t)$ are retrieved as a particular case of Proposition 3.1. The time evolution of $\sigma^2[g]$ reads

$$(3.23) \quad \frac{d}{dt} \sigma^2[g] = - \int_{\mathbb{R}^{2d}} |v - v_*|^2 P(v, v_*) g g_* dv dv_* - 2 \frac{k_d}{\nu} \varrho \sqrt{\sigma^2[g^0] \sigma^2[g]},$$

and the bounds for $\sigma^2[g](t)$ correspond to the estimate in (3.15) where now $\beta(t) \equiv 1$,

$$(3.24) \quad \sigma^2[g^0]e^{-2bt} \left(1 - \frac{1}{\nu} \int_0^t e^{bs} k_d(s) ds\right)^2 \leq \sigma^2[g](t) \leq \sigma^2[g^0]e^{2at} \left(1 + \frac{1}{\nu} \int_0^t e^{-as} k_d(s) ds\right)^2 \blacksquare$$

The loss of the exponential decay constitutes the main drawback of this approach, on the other hand we can still control the concentration of the density towards a reference solution.

3.2. Closed-loop Riccati control. We can carry out the derivation of the mean field limit performed in the previous section also for system (2.28). Introducing the mean field density $g(v, t)$, the mean field limit of (2.28) is

$$(3.25) \quad \partial_t g = -\nabla_v \cdot \left(g \left(\mathcal{P}[g] - \frac{k_d}{\nu} v - \frac{k_o}{\nu} m_1[g] \right) \right), \quad g(v, 0) = g^0(v)$$

where $m_1[g]$ indicates the average of the particle density $g(v, t)$

$$m_1[g](t) = \int_{\mathbb{R}^d} v g(t, v) dv,$$

where $k_o(t), k_d(t)$ are obtained by a Riccati system (3.4). In the next section we derive bounds on moments.

3.2.1. Bounds of decay moments. The first moment of (3.25) is the same as (3.10), and using the symmetry of the interaction kernel $P(\cdot, \cdot)$ we have

$$(3.26) \quad \frac{d}{dt} m_1[g](t) = -\frac{k_d + k_o}{\nu} m_1[g](t), \quad m_1[g](0) = m_1[g^0].$$

By a direct computation we get

$$(3.27) \quad \frac{d}{dt} m_2[g] = -\int_{\mathbb{R}^{2d}} |v - v_*|^2 P(v, v_*) g(v) g(v_*) dv dv_* - \frac{2}{\nu} (k_d m_2[g] + k_o |m_1[g]|^2),$$

and the variance equation

$$(3.28) \quad \frac{d}{dt} \sigma^2[g] = -\iint |v - v_*|^2 P(v, v_*) g(v) g(v_*) dv dv_* - \frac{2k_d}{\nu} \sigma^2[g].$$

LEMMA 3.2. *Assume $-a \leq P(v, w) = P(w, v) \leq b$ with $a, b > 0$, then there exists lower and upper bound for the variance of g*

$$(3.29) \quad \sigma^2[g^0]e^{-2bt} C_\nu(0, t) \leq \sigma^2[g](t) \leq \sigma^2[g^0]e^{2at} C_\nu(0, t).$$

where

$$C_\nu(0, t) = \exp \left\{ -\frac{2}{\nu} \int_0^t k_d(s) ds \right\}.$$

Proof. Since the interaction kernel is bounded $-a \leq P(v, w) \leq b$ and we have the identity

$$\iint |v - w|^2 g(v) g(v_*) dv dv_* = 2m_2[g] - 2|m_1[g]|^2 = 2\sigma^2[g],$$

it follows that

$$(3.30) \quad -2\left(b + \frac{k_d}{\nu}\right) \sigma^2[g] \leq \frac{d}{dt} \sigma^2[g] \leq 2\left(a - \frac{k_d}{\nu}\right) \sigma^2[g]. \quad \square$$

In Figure 3.3 the decay of the variance $\sigma^2[g]$ and the bounds associated to kernel (3.20) are shown. We choose the same parameters as reported in Figure 3.2. We observe that bounds of the closed-loop control (2.28) are closer compared to equation (2.30). Further, a stronger decay is observed. Hence, we expect better performances of the closed-loop control over the open-loop approaches. However the open-loop approach (2.30) turns to be useful when we are dealing with incomplete information or limited access to the non-linear dynamics.

We devote the next section to the development of a numerical procedure based on predictive horizons estimated a-priori by the bounds of the open-loop strategy (2.30).

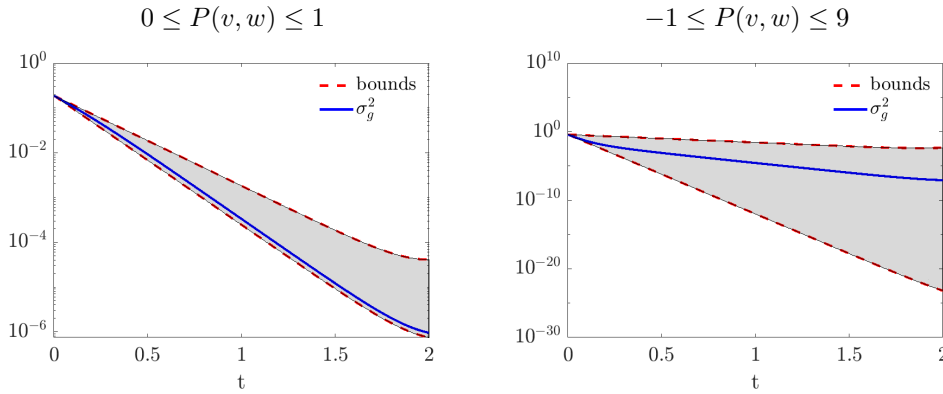


FIG. 3.3. Variance decay and bounds for the open-loop approach (2.28). On the left we observe the decay for an attractive dynamics, on the right the attractive-repulsive case.

4. Moment-driven predictive control (MdPC). In order to utilize the stabilization properties of the control loops proposed in the previous sections, we discuss their implementation in a receding horizon framework. Here, we prescribe a control horizon where the control signal is applied, after which there is an update procedure including a re-calculation of the control law based on the current state of the system. There exists a vast literature addressing the design of nonlinear model predictive control (MPC) algorithms, we refer the reader to [54, 45] and references therein.

In the general nonlinear MPC control algorithm, an open-loop optimal control signal is synthesized over a prediction horizon $[0, T_p]$, by solving a problem of the form (2.2). Having prescribed the system dynamics and the running cost, this optimization problem depends on the initial state $v(0)$ and the horizon T_p only. The optimal signal u^* , which is obtained for the whole horizon $[0, T_p]$, is implemented over a shorter control horizon $[0, T_c]$. At $t = T_c$ the initial state of the system is re-calibrated to $v(0) = v(T_c)$ and the optimization is repeated. Relevant issues in the MPC literature are the selection of suitable horizons T_p and T_c which can ensure asymptotic stability of the closed-loop, as well as the design of effective optimization methods to make this implementation suitable for real-time control.

Here instead, we propose a novel class of MPC-type algorithms where instead of fixing a prediction horizon, the re-calibration of the control laws (2.30)-(2.33) is triggered adaptively in time based on a direct estimate of the moments decay. This is similar in spirit to the literature on event-based MPC methods, see for example [36] where an event-based framework for the control of a team of cooperating distributed agents and [65] for networked systems is proposed.

Variance driven Predictive Control MdPC(σ^2). Starting from the open-loop control (3.6) we consider densities at initial time given by $g(v, 0) = g^0(v)$, $f^0(w) \equiv g^0(w)$ and the joint distribution $\lambda^0(v, w) \equiv \lambda(v, w, t_0)$. To shorten the notation we introduce the general semi-discretization of the mean-field dynamics (3.5) as follows

$$(4.1) \quad \lambda^{n+1}(v, w) = \Phi_{\Delta t}[\lambda^n; u^n[f^n]](v, w), \quad \lambda^0(v, w) = \lambda(v, w, 0), \quad n \geq 0,$$

coupled with the solution of the Riccati system (3.4). Here, $\Phi_{\Delta t}$ defines the time discretization, and $u^n[f^n]$ encodes the control depending on the density $f(w, t_n)$ defined as follows

$$(4.2) \quad u^n[f^n](w, t_n) = \frac{1}{\nu} (k_d(t_n)w + k_o(t_n)m_1[f^n](t_n)).$$

Our goal is to predict the error in the variance decay $\sigma^2[g](t)$ directly from (3.15) by computing the difference between the upper and lower bounds as follows

$$(4.3) \quad \Delta_\sigma(t_0, t) = \sigma^2[g(v, t_0)] \left[(e^{2a(t-t_0)} (1 + B_a^-(t_0, t))^2 - e^{-2b(t-t_0)} (1 - B_b^+(t_0, t))^2 \right],$$

where $B_c^\pm(t_0, t)$ are the quantities defined in (3.16). Then we can use $\Delta(t_0, t)$ to control the decay of the variance $\sigma^2[g](t)$ in order to keep the variance of $g(v, t)$ below a fixed threshold $\delta > 0$. In this way, we can find time $t_1 > t_0$ such that $\Delta(t_0, t_1) > \delta$ and evolve the dynamics in the time interval $[t_0, t_1]$. The procedure is reinitialized updating the state of the linearized dynamics at time t_1 by setting $f(t_1, v) \equiv g(t_1, v)$. We formalize this procedure in Algorithm 4.1.

Algorithm 4.1 [MdPC(σ^2)]

0. Set $k \leftarrow 0$, $t_k = 0$, $g^k(v) = g(v, 0)$, $f^k(v) = g(v, 0)$ and tolerance δ
1. Solve Riccati to obtain k_d, k_o on the time interval $[0, T]$
2. Find the time t_{k+1} such that

$$(4.4) \quad t_{k+1} := \min\{t | t_k < t \leq T, \Delta_\sigma(t_k, t) > \delta\}$$

while $t_{k+1} \leq T$ **do**

- i. Evolve the dynamics (4.1) up to t_{k+1}
- ii. Set $g_{k+1}(v) = g(v, t_{k+1})$, $f_{k+1}(v) = g(v, t_{k+1})$
- iii. $k \leftarrow k + 1$
- iv. Compute t_{k+1} from (4.4);

end while

Mean and variance driven predictive control, MdPC(m_1, σ^2). For the inexact open-loop control approach (3.9) it is necessary to modify the previous algorithm controlling also the decay of the first moment of $g = g(v, t)$. For this, we introduce the semidiscretized mean-field model of (3.9) as follows

$$(4.5) \quad \lambda^{n+1}(v, w) = \Phi_{\Delta t}[\lambda^n; u^n[g^0]](v, w), \quad \lambda^0(v, w) = \lambda(v, w, 0), \quad n \geq 0,$$

where the control is given by

$$(4.6) \quad u^n[g^0](w, t_n) = \frac{1}{\nu} (k_d(t_n)w + k_o(t_n)m_1[g^0]).$$

According to the bounds (3.24), the decay of the variance is controlled by $\Delta_\sigma(t_0, t)$ as in (4.3) with

$$(4.7) \quad B_c^\pm(t_0, t) = \frac{1}{\nu} \int_{t_0}^{t-t_0} k_d(s) e^{\pm c(s-t_0)} ds.$$

However, in this case the convergence towards the desired state is not guaranteed since the decay of the first moment (3.22) does not match the moment of the linearized model (3.6b). To guarantee consensus convergence we require (3.22) to be contractive. For this, we introduce the control quantity

$$(4.8) \quad \Delta_m(t_0, t) = \left| 1 - \frac{1}{\nu} \int_{t_0}^{t-t_0} (k_d(s) + k_o(s)) ds \right|, \quad 0 < \tau \leq 1,$$

which we use to determine updates in Algorithm 4.2.

Algorithm 4.2 [MdPC(m_1, σ^2)]

0. Set $k \leftarrow 0$, $t_k = 0$, $g^k(v) = g(v, 0)$ and tolerances $\delta, \tau > 0$
1. Solve Riccati to obtain k_d, k_o on the time interval $[0, T]$.
2. Find the times t_δ, t_τ such

$$(4.9) \quad \begin{aligned} t_\delta &:= \min\{t | t_k < t \leq T, \Delta_\sigma(t_k, t) > \delta\}, \\ t_\tau &:= \min\{t | t_k < t \leq T, \Delta_m(t_k, t) > \tau\}, \\ t_{k+1} &:= \min\{t_\delta, t_\tau\} \end{aligned}$$

while $t_{k+1} \leq T$ **do**

- i. Evolve the dynamics (4.5) up to t_{k+1}
- ii. Set $g^{k+1}(v) = g(v, t_{k+1})$ and $g^0(v) = g(v, t_{k+1})$
- iii. $k \leftarrow k + 1$
- iv. Compute t_{k+1} from (4.9);

end while

Remark 4.1. In this class of methods the main difference with respect to standard MPC techniques consists in the definition of control horizons. In the case of event-driven predictive control the control horizon is determined at the current time t_k based on estimates of the variance decay in (4.3).

We further observe that when an update is performed at each time step, that is for values of δ small enough, the MdPC approach is equivalent to a discretization of the closed-loop control (3.25). Indeed, since for every $n \geq 0$ $f^n \equiv g^n$, the mean-field model (4.1) collapses to

$$(4.10) \quad g^{n+1}(v) = \Phi_{\Delta t}[g^n; u[g^n]](v), \quad n \geq 0, \quad g^0(v) = g(v, t_0),$$

where the control is $u[g^n]$ is defined as

$$(4.11) \quad u[g^n](v, t_n) = \frac{1}{\nu} (k_d(t_n)v + k_o(t_n)m_1[g^n](t_n)).$$

5. Numerical Experiments. In this section we present different numerical tests on microscopic and mean field dynamics. We analyze three different cases:

a first order opinion dynamics, a second order alignment model, and first order aggregation model. For the numerical solution of the mean-field model (3.6) we employ mean-field Monte-Carlo methods (MFMCs) developed in [7]. These methods fall in the class of fast algorithms developed for interacting particle systems such as direct simulation Monte-Carlo methods (DSMCs) [15, 32, 11], or most recently Random Batch Methods (RBMs) [55].

We consider N_s particles $v^0 \equiv \{v_i^0\}_i$ sampled from the initial distribution $g^0(v)$, and we duplicate the sample defining $w^0 \equiv v^0$ for the linearized dynamics. We introduce the following approximation for the mean field dynamics

$$(5.1a) \quad v_i^{n+1} = (1 - \Delta t \hat{P}_i^n) v_i^n + \Delta t \hat{P}_i^n \hat{V}_i^n - \Delta t u_i^n,$$

$$(5.1b) \quad w_i^{n+1} = (1 - \Delta t \bar{p}) w_i^n + \Delta t \bar{p} \hat{m}_1^n - \Delta t u_i^n,$$

for $n \geq 0$ and where the quantities \hat{P}_i^n and \hat{V}_i^n are computed from a sub-sample of M particles randomly selected from the whole ensemble of N_s particles as follows

$$\hat{P}_i^n = \frac{1}{M} \sum_{k=1}^M P(v_i^n, v_{i_k}^n), \quad \hat{V}_i^n = \frac{1}{M} \sum_{k=1}^M \frac{P(v_i^n, v_{i_k}^n)}{\hat{P}_i^n} v_{i_k}^n, \quad i = 1, \dots, N_s.$$

For the open-loop mean field dynamics (4.1) the control u_i^n is defined as

$$(5.2) \quad u_i^n = -\frac{1}{\nu} (k_d^n w_i^n + k_o^n \hat{m}_1^n), \quad \hat{m}_1^n = \frac{1}{N_s} \sum_{j=1}^{N_s} w_j^n.$$

The scheme (5.1) reduces to a set of equations for the mean field dynamics for the closed-loop (4.10) and inexact open-loop (4.5), respectively. In the closed-loop setting (4.10) the control term is computed as

$$(5.3) \quad u_i^n = -\frac{1}{\nu} (k_d^n v_i^n + k_o^n \hat{m}_1^n), \quad \hat{m}_1^n = \frac{1}{N_s} \sum_{j=1}^{N_s} v_j^n,$$

in the inexact open-loop approach (4.5) we have

$$(5.4) \quad u_i^n = -\frac{1}{\nu} (k_d^n v_i^0 + k_o^n \hat{m}_1^0), \quad \hat{m}_1^0 = \frac{1}{N_s} \sum_{j=1}^{N_s} v_j^0.$$

We report in Table 5.1 the different choice of parameters used for the numerical discretization of the mean field dynamics and for each control approach, respectively. In order to compare the performances of the various control we consider the discretized cost functional $J(g, u)$

$$(5.5) \quad J_{\Delta t, N_s}(u, g^0) := \frac{\Delta t}{N_s} \sum_{n=0}^{N_T} \sum_{j=1}^{N_s} (|v_j^n|^2 + \nu |u_j^n|^2),$$

with time step Δt and N_s Monte Carlo samples.

5.1. Test 1: Opinion formation. We show an example in the context of opinion formation by Hegselmann-Krause [48]. We consider the positive interaction kernel defined as

$$P(v, w) = C \cdot \chi(|w - v| < \eta),$$

	N_s	M	Δt	ν	T	δ	τ
Opinion formation	1e4	100	1e-2	1e-2	1	1e-1	1
Cucker-Smale dynamics	1e5	100	5e-2	1e-1	3	1	N.A.
Aggregation dynamics	1e5	10	1e-2	1	7	1e-1	N.A.

TABLE 5.1

Parameters for the various computational tests.

where $\eta = 0.25$ represents the confidence level and with a constant $C = 10$. The initial density of particle $g^0(v)$ is chosen such that consensus towards the target $\bar{v} = 0$ would not be reached without control action, that is e.g.

$$g^0(v) = \frac{2}{3}\chi_{[1/4, 7/4]}(v).$$

Numerically we use the forward scheme (5.1) with fixed time step $\Delta t = 0.01$, sampling size $N_s = 10000$ of the initial distribution $g^0(v)$ and fixed $M = 100$ for the approximation of the non-local interactions. To compare the mean field dynamics with the microscopic we simulate $N = 50$ agents uniformly sampled from g^0 .

In the top row of Figure 5.4 the uncontrolled dynamics is shown, where clusters of opinions emerge due to structure of the interaction kernel P . The second and third row of Figure 5.4 depicts the controlled dynamics for the microscopic and the mean field dynamics: left column reports the MdPC(m_1, σ^2), central column the MdPC(σ^2) and right column the closed-loop control. The left column of Figure 5.4 illustrates the convergence to the target when the MdPC(m_1, σ^2) is applied. Algorithm 4.2 is used with δ and τ chosen according to Table (5.1). The vertical lines in the plots represent the times of the update. We have a different situation with the MdPC(σ^2) approach 4.1, depicted in the middle of Figure 5.4. In this case the control is applied by directly embedding the linear synthesis into the the non-linear dynamics. As a consequence we need also the evolution of the linear state that we plot in a dashed green line for the microscopic case. The right column of Figure 5.4 eventually reports the closed-loop control results.

We perform a numerical analysis to study the decay of the variance $\sigma^2[g]$ using different values of δ in Algorithm 4.1 and Algorithm 4.2.

Figure 5.5 compares the variance of the system as the values of the tolerance δ changes. It can be seen that as δ decreases, the MdPC(σ^2) approaches the closed-loop control approach. This numerical evidence is further confirmed by Table 5.2. With decreasing values of δ we have an increasing number of updates and the values of the functional $J_{\Delta t, N_s}$ computed in (5.5) is similar for the three control approaches.

Thus we observe that the closed-loop control is the limiting case of the moments driven MPC methods.

5.2. Test 2: Cucker-Smale dynamics. We show the case of alignment second order one dimensional model with Cucker-Smale type interaction [27]. We consider a state characterized by $(x_i, v_i) \in \mathbb{R}^2$. The interaction kernel is defined as follows

$$P(x, y) = \frac{1}{(1 + |y - x|^2)^\gamma}, \quad \gamma \geq 0,$$

which is a decreasing function of the relative distance and it is bounded in $[0, 1]$. Under the condition $\gamma \geq 1/2$ the system does not reach flocking state unconditionally of the initial state [27]. We set $\gamma = 2$ and a suitable initial state, such that the flocking

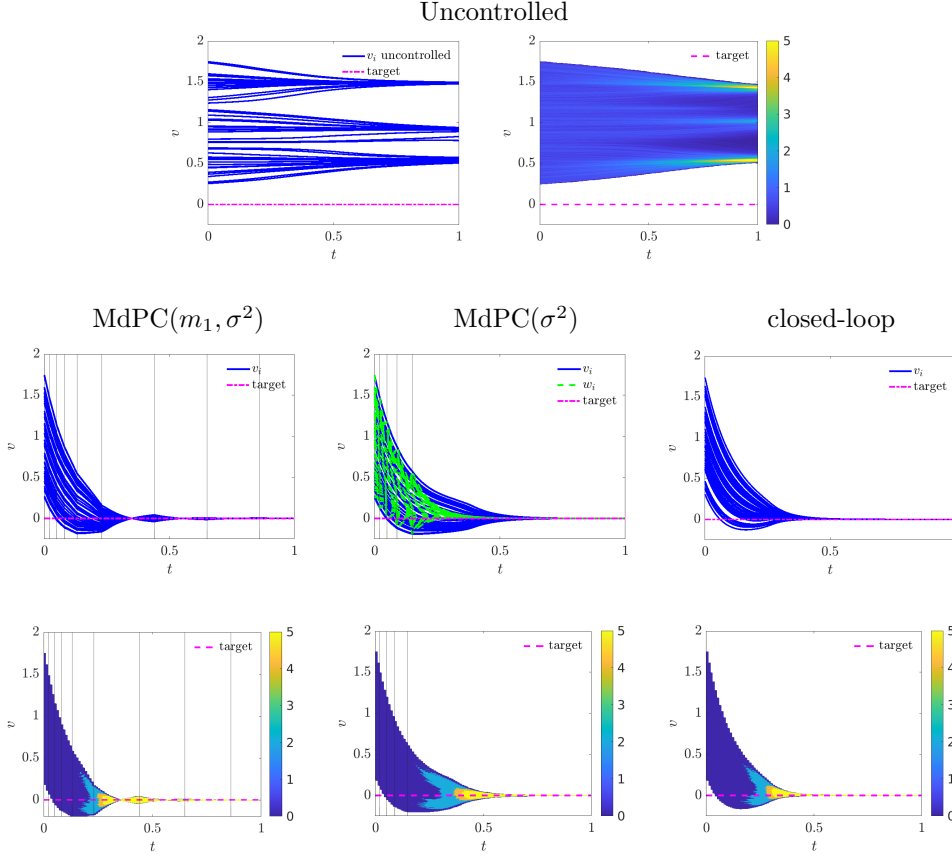


FIG. 5.4. Test 1: Opinion dynamics. *On the top the uncontrolled discrete and mean field evolution of the model. In the middle part the controlled discrete case and below the controlled meanfield dynamics. We show the three approaches, the inexact open-loop, the open-loop and the closed-loop respectively.*

	MdPC(m_1, σ^2)			MdPC(σ^2)			closed-loop
δ	1	0.1	1e-8	1	0.1	1e-8	--
update (%)	4 %	8%	71 %	0 %	4 %	72 %	100 %
$\sigma^2[g](T)$	1.28e-11	1.26e-10	3.80e-12	5.04e-2	8.94e-9	2.22e-12	2.22e-12
$J_{\Delta t, N_s}$	1.8131	0.1306	0.1281	0.1777	0.1309	0.1281	0.1281

TABLE 5.2

Test 1: Opinion dynamics. *We compare the different control approaches. For MdPC(m_1, σ^2) the tolerance for the mean is set $\tau = 1$, whereas δ varies. Number of updates indicates for MdPC methods the percentage of control updates over the total number of time steps $N_T = 100$. $\sigma^2(T)$ detects the final values of the variance for the density of particles $g(v, T)$. Finally $J_{\Delta t, N_s}$ reports the value of the cost functional (5.5).*

state is not achieved without control action. To perform our analysis we refer to the second order dynamics (2.24) and use Remark 2.1 to obtain the Riccati equations. Differently from first order dynamics, the constrained mean field has a transport term

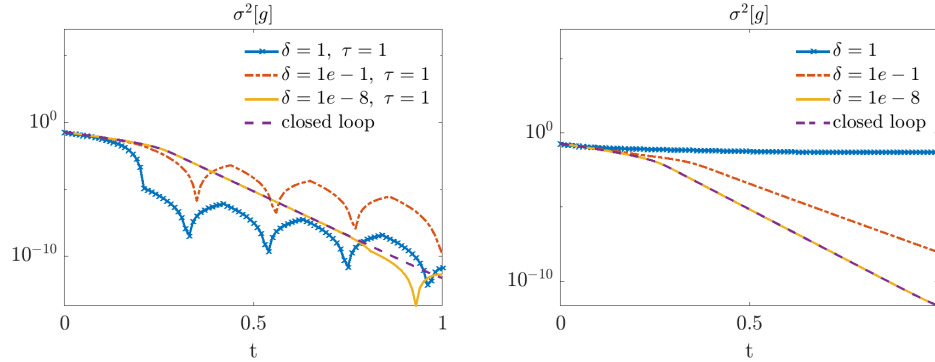


FIG. 5.5. Test 1: Opinion dynamics. *Semi-log plot with a comparison between variance decay with different values of the tolerance δ . On the left variance decays for $\text{MdPC}(m_1, \sigma^2)$, on the right decays for $\text{MdPC}(\sigma^2)$ compared with respect to the closed-loop control.*

as follows

$$(5.6) \quad \partial_t g + v \cdot \nabla_x g = -\nabla_v \cdot (g(\mathcal{P}[g] + u(t))), \quad g(x, v, 0) = g^0(x, v),$$

where $u(t)$ denotes the generic control strategy and the nonlocal operator \mathcal{P} is defined is

$$\mathcal{P}[g](x, v, t) = \int_{\mathbb{R}^d \times \mathbb{R}^d} P(x, y)(w - v)g(y, w, t) dy dw.$$

We discretize the mean field model employing the forward scheme (5.1) with fixed time step $\Delta t = 0.05$, sampling size of $N_s = 100000$ particles and fixed $M = 100$. In order to treat the additional transport term in the dynamics we use a splitting method to perform the free transport step. The control is computed by means of $\text{MdPC}(\sigma^2)$. We refer to Table (5.1) for the choice of parameters.

Figure 5.6 presents the initial data at the top, which is a bivariate distribution unimodal in space and bimodal in velocity defined as follows:

$$g^0(x, v) = \frac{1}{4\pi\sigma_x\sigma_v} \exp\left(-\frac{x^2}{2\sigma_x^2}\right) \left[\exp\left(-\frac{(v+v_-)^2}{2\sigma_v^2}\right) + \exp\left(-\frac{(v+v_+)^2}{2\sigma_v^2}\right) \right],$$

with $\sigma_x = 0.2, \sigma_v = 0.4$ and $v_- = -1, v_+ = 4$. We report as comparison the evolution of the density distribution in the phase space (x, v) , jointly with a set of $N = 30$ microscopic points $(x_i(t), v_i(t))$ sampled from the initial distribution. The middle row depicts two time frames of the uncontrolled dynamics, where alignment is not reached. In the bottom row we report the constrained dynamics, where the alignment is reached at time $T = 3$ and the density $g(x, v, t)$ concentrates at the target state $\bar{v} = 0$, whereas in space its support is bounded.

We perform a numerical study for the variance decay $\sigma^2[g]$ using different tolerances δ in Algorithm 4.1 for $\text{MdPC}(\sigma^2)$. Figure 5.7 compares the decay of the variance of the system as the values of the tolerance δ changes. On the left we observe the decay for $\delta = 1$ jointly with the update and the evolution of the variance bounds. On the right, it can be seen that as δ decreases $\text{MdPC}(\sigma^2)$ is similar to the closed-loop control dynamics. Table 5.3 quantifies the performances of the $\text{MdPC}(\sigma^2)$ reporting the percentage of control updates performed over $N_T = 60$ steps, the variance $\sigma^2[g]$ at time $T = 3$, and the value of the cost functional (5.5).

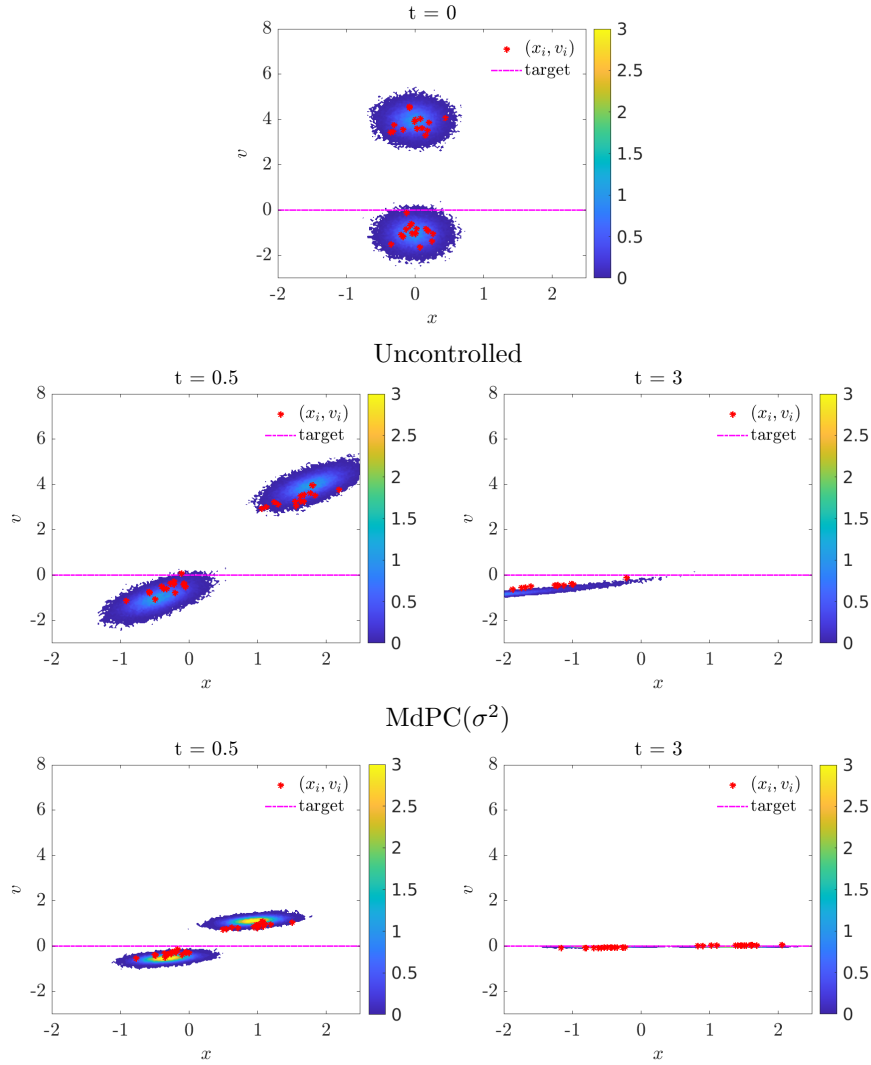


FIG. 5.6. Test 2: Cucker-Smale. Comparison between the uncontrolled and controlled mean field evolution of the Cucker-Smale dynamics with $\text{MdPC}(\sigma^2)$ and $\delta = 1$. Without control intervention the alignment state is not reached.

δ	$\text{MdPC}(\sigma^2)$			closed-loop
	1	1e-2	1e-8	--
update (%)	13 %	40 %	99 %	100%
$\sigma^2[g](T)$	9.1393e-05	3.9247e-08	3.3374e-08	3.3371e-08
$J_{\Delta t, N_s}$	3.0059	2.9976	2.9951	2.9951

TABLE 5.3

Test 2: Cucker-Smale. Number of updates and final values of the variance using different values of δ . We compare the different control approaches. The percentage of update is computed over the total number of time steps $N_T = 60$.

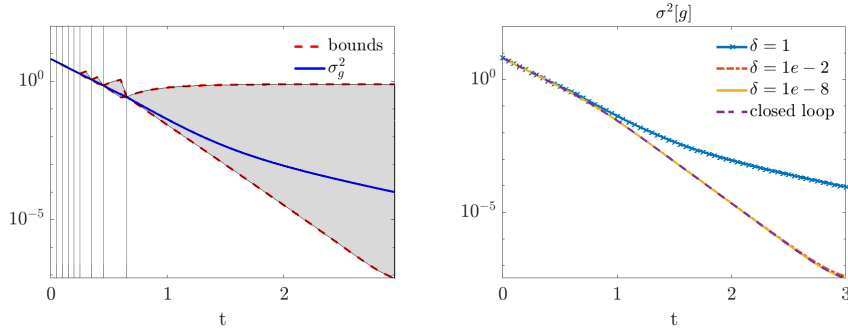


FIG. 5.7. Test 2: Cucker-Smale. *On the left the variance and bounds for the second order attractive one-dimensional mean field dynamics with tolerance $\delta = 1$. On the right a semi-log plot with a comparison between variance decay with different values of δ .*

5.3. Test 3: Aggregation dynamics. The last example is a first order aggregation model in 2D, where agents interact according to an attraction-repulsion kernel. We consider the following interaction kernel

$$P(v, w) = |w - v|^{\alpha-2} - |w - v|^{\beta-2},$$

where $\alpha = 4$ and $\beta = 2$. For these specific values of the parameters it can be shown that the equilibrium configuration is an uniform distribution on an annulus of radius $R = \frac{1}{\sqrt{3}}$ and same center as the initial distribution. For analytical and numerical characterization of the equilibrium of these models we refer to [13].

Thus we consider an initial density of particles uniformly distributed on the 2D disc of radius $R_0 = \frac{2}{\sqrt{3}}$ centered in $(-1, 1)$, as follows

$$(5.7) \quad g^0(v) = \frac{1}{|\mathcal{C}|} \chi_{\mathcal{C}}(v),$$

being $\mathcal{C} := \{v \in \mathbb{R}^2 : |v - (-1, 1)^\top| \leq R_0\}$, and $|\mathcal{C}|$ being its volume. In order to simulate the dynamics we consider $N_s = 100000$ particles sampled from $g^0(v)$ and we implement the forward scheme (5.1) with fixed time step $\Delta t = 0.01$. We select $M = 10$ particles for the approximation of the non local interactions. We use the MdPC(σ^2) approach with penalization factor $\nu = 1$ and a stopping tolerance $\delta = 0.1$. In Figure 5.8 we report the evolution of the mean field and the microscopic dynamics. The latter is sampled with $N = 30$ particles from g^0 . In the second row of Figure 5.4 shows the uncontrolled dynamics, where mass concentrates towards a 2D annulus of radius $R = \frac{1}{\sqrt{3}}$. While the third row depicts the open-loop control case where MdPC(σ^2) is applied. At time $T = 7$ the distribution is converged to a concentration at $\bar{v} = (\bar{v}_1, \bar{v}_2) = (0, 0)$.

As in previous tests we illustrates a comparison between different open-loop controls varying tolerance δ in algorithms 4.1. Figure 5.9 and Table 5.4 highlight that with a very small value of δ , the MdPC approach coincides with the closed-loop approach.

Concluding Remarks. We have studied the design of control laws for interacting particle system based on the solution of the optimal control problem associated to linearized dynamics. In this paper we have assessed the impact of different sub-optimal control laws into the original non-linear dynamics deriving mean field limits of the microscopic constrained systems and estimating analytically and numerically

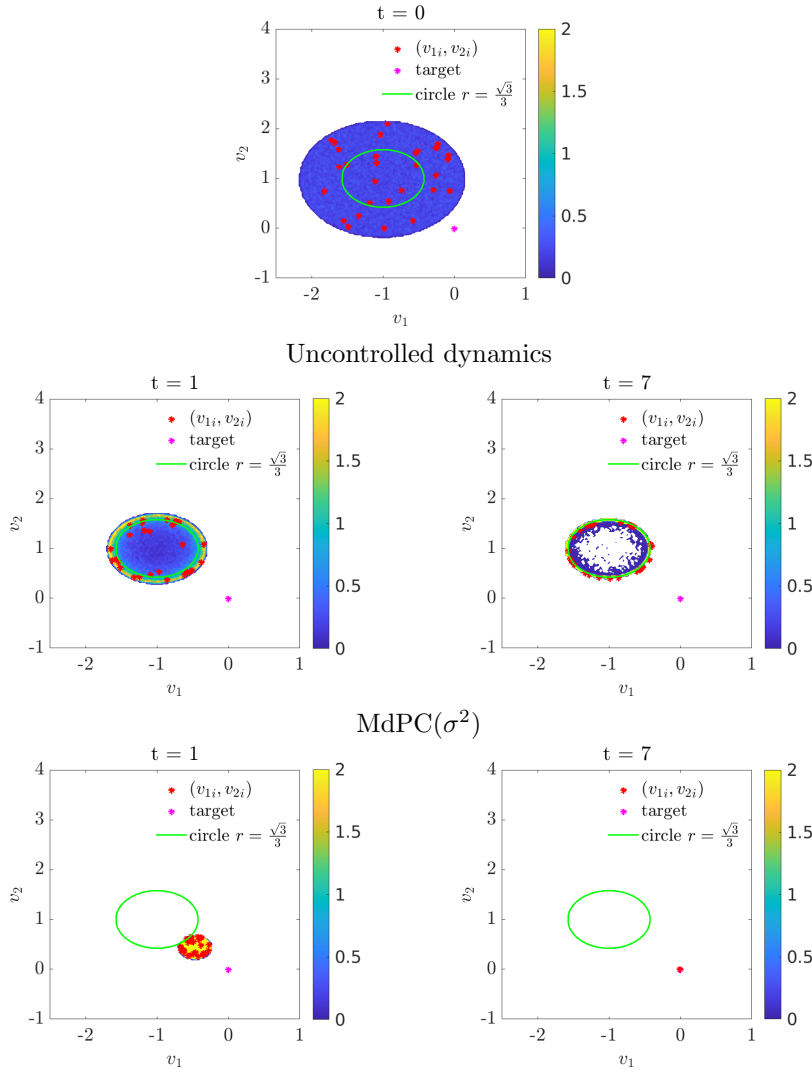


FIG. 5.8. Test 3: Aggregation dynamics. Comparison between the uncontrolled and controlled mean field evolution of the aggregation dynamics with $MdPC(\sigma^2)$ and $\delta = 0.1$. Without control intervention the alignment state is not reached.

	MdPC(σ^2)			closed-loop
δ	1	1e-1	1e-9	--
update (%)	1 %	4 %	99 %	100%
$\sigma^2[g](T)$	1.6875e-09	2.1253e-08	2.6151e-08	2.6187e-08
$J_{\Delta t, N_s}$	3.0459	2.9751	2.9750	2.9750

TABLE 5.4

Test 3: Aggregation dynamics. Number of updates and final values of the variance using different values of δ . The percentage of update is computed over the total number of time steps $N_T = 700$.

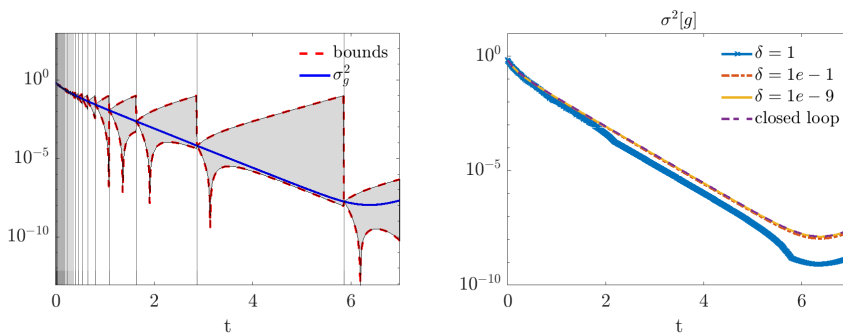


FIG. 5.9. Test 3: Aggregation dynamics. *On the left the variance evolution and bounds for the first order attractive-repulsive one-dimensional meanfield dynamics with tolerance $\delta = 0.1$. On the right a semi-log plot with a comparison between variance decay with different values of δ .*

the decay of the first and second moments. We proposed a novel numerical technique based on the moments decay (MdPC). In particular, we obtain a hierarchy of approximations from open-loop to closed-loop control by scaling the tolerance level. These strategies have shown to be robust even with only a few updates of the control law for the non-linear dynamics. The proposed methodology expands the existing NMPC literature by developing a new paradigm in which the control laws are updated based on dynamic information of the system. Here, the use of moments information is a particular example suitable in the context of mean-field dynamics. Further extensions and analysis will include the study of other dynamic indicators for control update, in particular those that could be linked to a physical observable of the system, and the incorporation of nonlinear state estimation in the control loop.

REFERENCES

- [1] M. Aduamoah, B. D. Goddard, J. W. Pearson, and J. C. Roden. Pde-constrained optimization models and pseudospectral methods for multiscale particle dynamics, 2020.
- [2] G. Albi, N. Bellomo, L. Fermo, S.-Y. Ha, J. Kim, L. Pareschi, D. Poyato, and J. Soler. Vehicular traffic, crowds, and swarms: from kinetic theory and multiscale methods to applications and research perspectives. *Math. Models Methods Appl. Sci.*, 29(10):1901–2005, 2019.
- [3] G. Albi, M. Bongini, E. Cristiani, and D. Kalise. Invisible control of self-organizing agents leaving unknown environments. *SIAM J. Appl. Math.*, 76(4):1683–1710, 2016.
- [4] G. Albi, Y.-P. Choi, M. Fornasier, and D. Kalise. Mean field control hierarchy. *Appl. Math. Optim.*, 76(1):93–135, 2017.
- [5] G. Albi, M. Herty, and L. Pareschi. Kinetic description of optimal control problems and applications to opinion consensus. *Commun. Math. Sci.*, 13(6):1407–1429, 2015.
- [6] G. Albi and D. Kalise. (sub)optimal feedback control of mean field multi-population dynamics. *IFAC-PapersOnLine*, 51(3):86 – 91, 2018. 6th IFAC Workshop on Lagrangian and Hamiltonian Methods for Nonlinear Control LHMNC 2018.
- [7] G. Albi and L. Pareschi. Binary interaction algorithms for the simulation of flocking and swarming dynamics. *Multiscale Model. Simul.*, 11(1):1–29, 2013.
- [8] G. Albi, L. Pareschi, and M. Zanella. Boltzmann-type control of opinion consensus through leaders. *Philos. Trans. R. Soc. Lond. Ser. A Math. Phys. Eng. Sci.*, 372(2028):20140138, 18, 2014.
- [9] B. Azmi, D. Kalise, and K. Kunisch. Data-driven recovery of optimal feedback laws through optimality conditions and sparse polynomial regression, 2020.
- [10] B. Azmi and K. Kunisch. A hybrid finite-dimensional RHC for stabilization of time-varying parabolic equations. *SIAM J. Control Optim.*, 57(5):3496–3526, 2019.
- [11] H. Babovsky and H. Neunzert. On a simulation scheme for the boltzmann equation. *Math. Methods Appl. Sci.*, 8(1):223–233, 1986.

- [12] R. Bailo, M. Bongini, J. A. Carrillo, and D. Kalise. Optimal consensus control of the cucker-smale model. *IFAC-PapersOnLine*, 51(13):1–6, 2018. 2nd IFAC Conference on Modelling, Identification and Control of Nonlinear Systems MICNON 2018.
- [13] D. Balagué, J. A. Carrillo, T. Laurent, and G. Raoul. Nonlocal interactions by repulsive-attractive potentials: radial ins/stability. *Phys. D*, 260:5–25, 2013.
- [14] N. Bellomo and J. Soler. On the mathematical theory of the dynamics of swarms viewed as complex systems. *Math. Models Methods Appl. Sci.*, 22(suppl. 1):1140006, 29, 2012.
- [15] A. Bobylev and K. Nanbu. Theory of collision algorithms for gases and plasmas based on the Boltzmann equation and the Landau-Fokker-Planck equation. *Phys. Rev. E*, 61(4):4576, 2000.
- [16] L. Boudin and F. Salvarani. A kinetic approach to the study of opinion formation. *M2AN Math. Model. Numer. Anal.*, 43(3):507–522, 2009.
- [17] A. Bressan and B. Piccoli. *Introduction to the mathematical theory of control*, volume 1. American institute of mathematical sciences Springfield, 2007.
- [18] L. M. Briceño Arias, D. Kalise, and F. J. Silva. Proximal methods for stationary mean field games with local couplings. *SIAM J. Control Optim.*, 56(2):801–836, 2018.
- [19] M. Burger, R. Pinnau, C. Totzeck, O. Tse, and A. Roth. Instantaneous control of interacting particle systems in the mean-field limit. *J. Comput. Phys.*, 405:109181, 20, 2020.
- [20] E. F. Camacho and C. B. Alba. *Model predictive control*. Springer Science & Business Media, 2013.
- [21] J. A. Canizo, J. A. Carrillo, and J. Rosado. A well-posedness theory in measures for some kinetic models of collective motion. *Math. Models Methods Appl. Sci.*, 21(03):515–539, 2011.
- [22] M. Caponigro, M. Fornasier, B. Piccoli, and E. Trélat. Sparse stabilization and control of alignment models. *Math. Models Methods Appl. Sci.*, 25(3):521–564, 2015.
- [23] J. A. Carrillo, Y.-P. Choi, and M. Hauray. The derivation of swarming models: mean-field limit and Wasserstein distances. In *Collective dynamics from bacteria to crowds*, pages 1–46. Springer, 2014.
- [24] Y.-P. Choi, D. Kalise, J. Peszek, and A. A. Peters. A collisionless singular Cucker-Smale model with decentralized formation control. *SIAM J. Appl. Dyn. Syst.*, 18(4):1954–1981, 2019.
- [25] S. Cordier, L. Pareschi, and G. Toscani. On a kinetic model for a simple market economy. *J. Stat. Phys.*, 120(1-2):253–277, 2005.
- [26] E. Cristiani, B. Piccoli, and A. Tosin. *Multiscale modeling of pedestrian dynamics*, volume 12 of *MSE&A. Model. Simul. Appl.* Springer, Cham, 2014.
- [27] F. Cucker and S. Smale. Emergent behavior in flocks. *IEEE Trans. Automat. Control*, 52(5):852–862, 2007.
- [28] P. Degond, S. Göttlich, M. Herty, and A. Klar. A network model for supply chains with multiple policies. *Multiscale Model. Simul.*, 6(3):820–837, 2007.
- [29] P. Degond, M. Herty, and J.-G. Liu. Flow on sweeping networks. *Multiscale Model. Simul.*, 12(2):538–565, 2014.
- [30] P. Degond, J.-G. Liu, S. Motsch, and V. Panferov. Hydrodynamic models of self-organized dynamics: derivation and existence theory. *Methods Appl. Anal.*, 20(2):89–114, 2013.
- [31] P. Degond and S. Motsch. Continuum limit of self-driven particles with orientation interaction. *Math. Models Methods Appl. Sci.*, 18(suppl.):1193–1215, 2008.
- [32] G. Dimarco, R. Caflisch, and L. Pareschi. Direct simulation Monte Carlo schemes for coulomb interactions in plasmas. *Commun. Appl. Ind. Math.*, 1(1):72–91, 2010.
- [33] S. Dolgov, D. Kalise, and K. Kunisch. Tensor decompositions for high-dimensional hamilton-jacobi-bellman equations, 2019.
- [34] J. R. Dyer, A. Johansson, D. Helbing, I. D. Couzin, and J. Krause. Leadership, consensus decision making and collective behaviour in humans. *Philos. Trans. Roy. Soc. B*, 364(1518):781–789, 2009.
- [35] M. R. D’Orsogna, Y.-L. Chuang, A. L. Bertozzi, and L. S. Chayes. Self-propelled particles with soft-core interactions: patterns, stability, and collapse. *Phys. Rev. Lett.*, 96(10):104302, 2006.
- [36] A. Eqtami, D. V. Dimarogonas, and K. J. Kyriakopoulos. Event-based model predictive control for the cooperation of distributed agents. In *2012 Amer. Control Conf. (ACC)*, pages 6473–6478, 2012.
- [37] G. Estrada-Rodriguez and H. Gimperlein. Interacting particles with Lévy strategies: limits of transport equations for swarm robotic systems. *SIAM J. Appl. Math.*, 80(1):476–498, 2020.
- [38] M. Fornasier, J. Haskovec, and G. Toscani. Fluid dynamic description of flocking via the Povzner-Boltzmann equation. *Phys. D*, 240(1):21–31, 2011.

- [39] M. Fornasier, S. Lisini, C. Orrieri, and G. Savaré. Mean-field optimal control as gamma-limit of finite agent controls. *European J. Appl. Math.*, 30(6):1153–1186, 2019.
- [40] M. Fornasier, B. Piccoli, and F. Rossi. Mean-field sparse optimal control. *Philos. Trans. R. Soc. Lond. Ser. A Math. Phys. Eng. Sci.*, 372(2028):20130400, 21, 2014.
- [41] M. Fornasier and F. Solombrino. Mean-field optimal control. *ESAIM Control Optim. Calc. Var.*, 20(4):1123–1152, 2014.
- [42] G. Freudenthaler and T. Meurer. PDE-based multi-agent formation control using flatness and backstepping: analysis, design and robot experiments. *Automatica J. IFAC*, 115:108897, 13, 2020.
- [43] J. Garnier, G. Papanicolaou, and T.-W. Yang. Consensus convergence with stochastic effects. *Vietnam J. Math.*, 45(1-2):51–75, 2017.
- [44] J. Gómez-Serrano, C. Graham, and J.-Y. Le Boudec. The bounded confidence model of opinion dynamics. *Math. Models Methods Appl. Sci.*, 22(2):1150007, 46, 2012.
- [45] L. Grüne and J. Pannek. Nonlinear model predictive control. In *Nonlinear model predictive control*, pages 45–69. Springer, 2017.
- [46] S.-Y. Ha and E. Tadmor. From particle to kinetic and hydrodynamic descriptions of flocking. *Kinet. Relat. Models*, 1(3):415–435, 2008.
- [47] Y. Han, A. Hegyi, Y. Yuan, S. Hoogendoorn, M. Papageorgiou, and C. Roncoli. Resolving freeway jam waves by discrete first-order model-based predictive control of variable speed limits. *Transportation Research Part C: Emerging Technologies*, 77:405–420, 2017.
- [48] R. Hegselmann, U. Krause, et al. Opinion dynamics and bounded confidence models, analysis, and simulation. *Journal of artificial societies and social simul.*, 5(3), 2002.
- [49] M. Herty and D. Kalise. Suboptimal nonlinear feedback control laws for collective dynamics. In *2018 IEEE 14th Intern. Conf. on Control and Automat. (ICCA)*, pages 556–561. IEEE, 2018.
- [50] M. Herty and L. Pareschi. Fokker-Planck asymptotics for traffic flow models. *Kinet. Relat. Models*, 3(1):165–179, 2010.
- [51] M. Herty, L. Pareschi, and S. Steffensen. Mean-field control and Riccati equations. *Netw. Heterog. Media*, 10(3):699, 2015.
- [52] M. Herty and C. Ringhofer. Averaged kinetic models for flows on unstructured networks. *Kinet. Relat. Models*, 4(4):1081–1096, 2011.
- [53] M. Herty and C. Ringhofer. Feedback controls for continuous priority models in supply chain management. *Comput. Methods Appl. Math.*, 11(2):206–213, 2011.
- [54] M. Herty and M. Zanella. Performance bounds for the mean-field limit of constrained dynamics. *Discrete Contin. Dyn. Syst.*, 37(4):2023, 2017.
- [55] S. Jin, L. Li, and J.-G. Liu. Random Batch Methods (RBM) for interacting particle systems. *J. Comput. Phys.*, 400:108877, 2020.
- [56] S. Liu, M. Jacobs, W. Li, L. Nurbekyan, and S. J. Osher. Computational methods for nonlocal mean field games with applications, 2020.
- [57] D. Q. Mayne, J. B. Rawlings, C. V. Rao, and P. O. Scokaert. Constrained model predictive control: Stability and optimality. *Automatica*, 36(6):789–814, 2000.
- [58] S. Motsch and E. Tadmor. Heterophilious dynamics enhances consensus. *SIAM review*, 56(4):577–621, 2014.
- [59] K.-K. Oh, M.-C. Park, and H.-S. Ahn. A survey of multi-agent formation control. *Automatica J. IFAC*, 53:424–440, 2015.
- [60] A. A. Peters, R. H. Middleton, and O. Mason. Leader tracking in homogeneous vehicle platoons with broadcast delays. *Automatica J. IFAC*, 50(1):64–74, 2014.
- [61] M. Petrovitch. Sur une manière d’étendre le théorème de la moyenne aux équations différentielles du premier ordre. (mit 2 figuren im text). *Mathematische Annalen*, 54:417–436, 1901.
- [62] R. E. Stern, S. Cui, M. L. Delle Monache, R. Bhadani, M. Bunting, M. Churchill, N. Hamilton, H. Pohlmann, F. Wu, B. Piccoli, et al. Dissipation of stop-and-go waves via control of autonomous vehicles: Field experiments. *Transp. Research Part C: Emerging Techn.*, 89:205–221, 2018.
- [63] G. Toscani. Kinetic models of opinion formation. *Commun. Math. Sci.*, 4(3):481–496, 2006.
- [64] A. Tosin and M. Zanella. Kinetic-controlled hydrodynamics for traffic models with driver-assist vehicles. *Multiscale Model. Simul.*, 17(2):716–749, 2019.
- [65] P. Varutti, B. Kern, T. Faulwasser, and R. Findeisen. Event-based model predictive control for networked control systems. In *Proc. of the 48th IEEE Conf. on Decision and Control (CDC) held jointly with 2009 28th Chinese Control Conf.*, pages 567–572, 2009.